

A status quo in aerial photogrammetric mapping

Fabio Remondino¹, Marc Muick², Michael Cramer³, Konrad Wenzel⁴, Klaus Legat⁵

¹ 3D Optical Metrology (3DOM) unit, Bruno Kessler Foundation (FBK), Trento, Italy - Email: remondino@fbk.eu

² Vexcel Imaging GmbH, Graz, Austria - Email: marc.muick@vexcel-imaging.com

³ Institute fuer Photogrammetrie und Geoinformatik, University of Stuttgart, Germany - Email: michael.cramer@ifp.uni-stuttgart.de

⁴ ESRI - Email: kwenzel@esri.com

⁵ AVT-Airborne Sensing Austria GmbH, Imst, Austria - Email: k.legat@avt.at

Keywords: photogrammetry, oblique, calibration, triangulation, DSM, LiDAR, hybrid

Abstract

Aerial photogrammetric 3D mapping refers to the process of capturing overlapping imagery - and increasingly, LiDAR data - via aerial platforms such as unmanned and manned aircraft, followed by computational processing to generate precise 3D representations of urban environments, infrastructure and natural landscapes. In recent years, the field has undergone significant transformation, driven by advancements in imaging technology, including larger and more sensitive sensors, the deployment of multi-camera systems and the integration of photogrammetry with LiDAR. These developments have been accompanied by increasing automation in feature detection, semantic segmentation and both 2D and 3D object classification. This paper aims to provide a critical review of the current state-of-the-art in sensor technologies and multi-sensor integration strategies. It highlights key technological innovations and evolving methodologies that are reshaping aerial 3D mapping practices and influencing both industry standards and market dynamics.

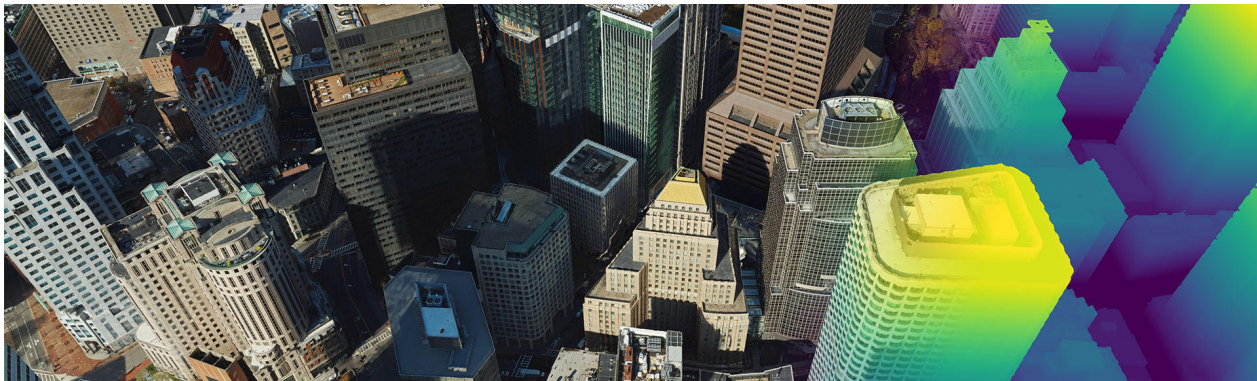


Figure 1. 3D mesh product from the Leica City Mapper 2 hybrid airborne sensor (4.5 cm GSD) - courtesy of Bluesky Ltd.

1. Introduction

Aerial photogrammetry and Airborne Laser Scanning (ALS) technologies (often called LiDAR) are consolidated and state-of-the-art solutions for aerial surveying applications (Kocaman et al., 2022). Drones and airborne platforms are being more and more equipped with high-resolution RGB, multispectral, hyperspectral and thermal cameras, LiDAR sensors or a combination of them. This allows detailed analyses and mapping outcomes for precision agriculture, smart forestry, environmental monitoring, infrastructure inspection, digital twins of cities, cartography update, quantitative assessment of the damages, etc. (Poli et al., 2017; Goodbody et al., 2019; Megahed et al., 2021; Lehtola et al., 2022).

Sensor selection is a critical component in airborne mapping, as it directly influences the quality and reliability of acquired data and delivered geospatial products. The optimal choice of the acquisition sensor is determined by several technical parameters, including project extent, spatial resolution requirements, desired level of detail, positional accuracy, sensor efficiency and budgetary constraints.

In parallel, recent improvements in photogrammetric and computer vision algorithms allow the creation of dense image matching (DIM) results (Remondino et al., 2014; Stathopoulou and Remondino, 2023). Image-based point clouds can have a spatial resolution equal to the image GSD (ground sample

distance) and an ideal accuracy at GSD level. Additionally, the inclusion of oblique images in the block enhances the overall triangulation and dense matching quality (Rupnik et al., 2015). The recent introduction to the market of hybrid systems combining active and passive sensors (Toschi et al., 2019; Bacher, 2022; Farella et al., 2025) is opening new scenarios in the airborne mapping and geospatial fields, with the opportunity to leverage each solution's strengths while mitigating their respective limitations. While LiDAR technologies stand out for the quality and reliability of height information, rapid acquisition of large volumes of data and ability to penetrate vegetation, photogrammetric data derived from high-resolution imagery excel for radiometric properties as well as highly detailed and accurate surface representation. So far, only a few hybrid orientation approaches of LiDAR and photogrammetric data have been presented (Glira et al., 2019; Haala et al., 2022; Jonassen et al., 2023; Mouzakidou et al., 2024). In most of the cases, the LiDAR strip adjustment and the aerial triangulation are separate processes and the data fusion is performed only at a later stage, limiting the potential benefits of hybrid systems in minimizing inconsistent data registration.

1.1 Aim of the work

While recent technological advancements in sensors and processing methods are evident in all fields, there is a clear need to report trends and examine geometric and radiometric

properties of actual aerial mapping cameras in the geospatial sector. The paper wants therefore to shed some light on the recent developments in aerial 3D mapping, reporting examples and experiences, specifically considering trends in sensor technologies (e.g. smaller pixel sizes, larger sensors, etc. – Section 2) and sensor integration (oblique and hybrid sensors – Section 3 and 4).

2. Trends in sensor technologies

2.1 Sensor design concepts

A key difference in current airborne camera design lies in the image composition, specifically how large format images are derived combining images from multiple smaller-format cameras. Three different generic approaches are used (Figure 2). In all cases, the large-format image is composed of multiple smaller images in so-called multi-head constellations but the difference lies in the arrangement of the individual sensors.

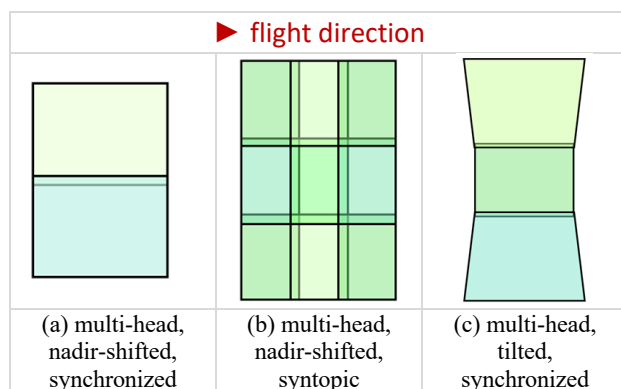


Figure 2. The basic concepts of large format imaging in mapping cameras through image composition.



Figure 3. Examples of centred (left) and shifted (right) focal plane (right), together with imaging rays and perspective centres.

Multi-head, nadir-shifted, synchronized (Figure 2a). Nadir-oriented camera sensors are arranged with certain shifts in their focal planes in order to have a wider coverage on the ground. The shifted frame approach can be well explained with Figure 3 that reports two camera heads from different Phase One cameras. In the right camera, the focal plane is shifted by a certain offset relative to the optics. Reconstructing the path of the imaging rays reveals that for the shifted camera head, the rays are directed to the right, whereas for the regular camera head, the rays pass symmetrically through the optics. If two such shifted camera heads are now arranged next to each other, a wider strip coverage

is obtained with still nadir-oriented viewing axes. The nadir parts of the Phase One PAS880 camera uses such combination of two shifted lens camera heads.

A certain challenge of this technology is that the relevant rays also pass through the lateral areas of the lenses, which places higher demands on the lens quality.

Multi-head, nadir-shifted, syntopic (Figure 2b). The shifted frame concept can also be combined with a time-delayed method, like in the Vexcel Ultracam series. Four camera heads aligned in flight direction are used to compose the large format nadir looking image. Due to the spatial distance of the respective camera heads, each camera head is triggered with a varying delay in the magnitude of a few milliseconds depending on its position. This results in almost identical perspective centers, and thus, ideally, each partial image has the same perspective. Different to the mostly applied synchronous imaging, where different camera heads are triggered at the same time, this delayed exposure concept is called syntopic imaging, as camera heads are exposed at the (almost) same position. One to four smaller format sensors are arranged in each of the camera heads. The master cone, with four sensors in the corners, defines the maximum extension of the focal plane. The remaining image parts captured by the three slave cones are stitched in the focal plane defined by the master cone.

Multi-head, tilted, synchronized (Figure 2c). The concept of working with tilted camera heads to cover a larger area is realized with one nadir and two (or more) tilted camera heads. This is currently utilized by IGI Urbanmapper and Leica Geosystems DMC-4 cameras, with the cameras next to the nadir cone tilted of $\pm 23\text{deg}$ (Urbanmapper-2) and $\pm 19\text{deg}$ (DMC-4). The tilting angles are always dependent on individual design of specific camera set-up, i.e. the focal length / lens opening angle of selected camera heads. The large format image is obtained by stitching the three individual camera heads. The PhaseOne Pana camera additionally incorporates two further tilted cameras to the right and left ($\pm 13\text{deg}$ and $\pm 27\text{deg}$), enabling even wider swaths (Jacobsen et al. 2025). In contrast to the oblique cameras, the tilting angles here are well below 45deg to minimize perspective differences caused by the tilt.

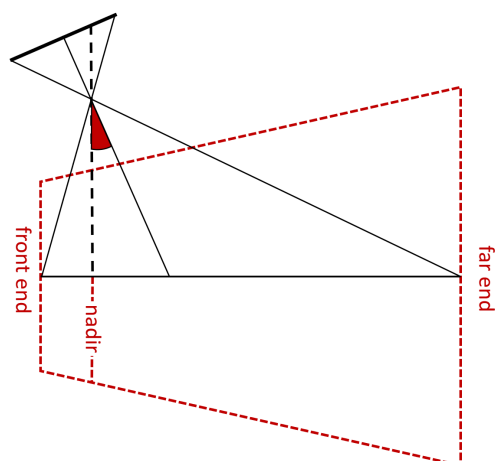


Figure 4: Image scale / GSD variation for a tilted camera head.

Tilt angle [deg]	15	20	25	45
GSD [cm] Nadir	10	10	10	10
GSD [cm] Front end	9.7	9.7	9.9	11.2
GSD [cm] Far end	11.2	11.8	12.7	19.4
Change [mm %]	15	21	28	81

Table 1. Variations in image scale / GSD for different tilt angles of camera heads.

Due to the tilt of the optics, perspective produces scale differences across the tilt axis (i.e. the axis around which the camera is rotated), which affects the GSD. Figure 4 and Table 1 report the influence of camera tilt on the GSD for a simulated camera head with focal length of 100 mm, a sensor side length of 53.4 mm and a flying height above ground of 2670 m. It is clear that with an increase of the camera tilt, the variation of the GSD from the near part of the image to the far part increases. For a 20 deg tilt angle, as it is common for most of the multi-head large image constellations, the variation of the GSD is in the range of 20% compared to the nadir point. Therefore, in stitching processes, i.e., when generating the virtual large format image, the composition plane and the resolution must be properly defined. The resolution can thus be calculated, for example, at the nadir point or, for example, based on the centre of the tilted camera head.

2.2 Smaller pixels

Actual sensors in photogrammetric aerial cameras are having smaller and smaller pixels (from 9-12 μm in early 2000s to 3 μm and below nowadays). This trend of using smaller pixels is dictated by collection efficiency which, on the other hand, results in higher flight altitudes due to focal length limitations (Table 2). These limitations can be understood as the necessity to stick to a certain focal length to restrict leaning effects to a usable amount. Furthermore, smaller pixels pose a significant challenge for optic design when the goal is to fully resolve the sensor pixels. Space constrains in aerial cameras are the main reason for this challenge. Another effect that needs to be discussed is atmospheric influence. Due to smaller pixel sizes, higher spatial frequencies must be resolved by the lens and also reach the sensor. However, atmospheric turbulences have a dampening effect that intensifies with increasing spatial frequency, leading to a reduction in image quality. The magnitude of this influence can be analysed by using the wavefront error. A smaller physical pixel size comes with the challenge of fewer photons reaching the reduced area, decreasing signal intensity. But this is generally largely compensated by improved sensor technology. For example, when comparing latest Sony's IMX 811 sensor (2.81 μm pixel size) with its predecessor IMX 411 (3.76 μm pixel size), based on real world measurements in a controlled environment with identical hardware (lenses), identical aperture and exposure time settings over the identical light source, it resulted that the recent IMX 811 is roughly only some 10% less light sensitive across the visible and near-infrared spectrum. During flight testing, it resulted that the 10% reduction in sensitivity corresponds to ca 3dB difference in signal-to-noise ratio, equivalent to half a bit of data in a raw image, hence a neglectable difference. This is not surprising because the final image quality is dependent on multiple factors such as sensor quality, lens quality, atmospheric effects, method of motion compensation and flying altitude.

Pixel size [μm]	Flight height [m] for 5 cm GSD	Flight height [m] for 10 cm GSD
9	556	1111
7.2	694	1389
6	833	1667
5.2	962	1923
4	1250	2500
3.76	1330	2660
2.81	1779	3559

Table 2. Relations between sensor's pixel size and flight altitudes for a 100 mm focal length lens to achieve 5 cm and 10 cm GSD.

2.2 Larger format sensors and focal lengths

In 20 years time, airborne camera sensors evolved from about 100 Mpx to over 500 Mpx for nadir frames, enabling the efficiency required for the increased demand in resolution, overlap and update time. For efficiency reasons, a wide swath is necessary to reduce the amount of flight lines and respect time and cost key factors in data acquisition. At the same time, opening angles need to be limited to achieve a balance between building lean in the image corners, while maintaining stereo capability for manual or automatic depth extraction (Poli et al., 2017). For this purpose, longer focal lengths (both the physical lens and also through smaller sensor pixels) are used today in common missions, e.g. 90-120 mm with ca 3 μm sensors. This allows a balance between small perspective distortion achieving high completeness in DSM and ortho production, while achieving a sufficient base-to-height ratio (image-ray intersection angle on the ground) for accurate height measurements. In case of pure ortho production without the need for DSMs/stereo or specific circumstances, very long focal lengths (e.g. 200 mm) are used, e.g. accommodating for flight restrictions over densely crowded airports. Very short focal lengths (e.g. 70 mm) are also just used for specific circumstances, e.g. flight restrictions or atmospheric limitations. Hence, balanced focal lengths close to the theoretical optimum of square root of 2, are recommended for optimal results both on the DSM depth accuracy as well as the ortho.

2.3 From pan-sharpening to Bayer pattern

The last years have seen a renaissance of Bayer filters in photogrammetric aerial camera. The advantage is compact manufacturing and costs reduction, although a slight reduction in image resolution and quality compared to a panchromatic sensor needs to be expected, as already reported in Remondino et al. (2016). The form factor is key for assembling large camera rigs, optionally including oblique views, while maintaining more unified components and allowing to fast swap / repair individual cones. Since Bayer pattern sensors were already used in multiple aerial camera systems to enable oblique view capabilities due to their smaller form factor, the new spreading trend is to use multiple – and mostly stitched – smaller-format Bayer pattern sensors to create large nadir footprints. This was fuelled simply by the availability of these sensors, the general trend towards efficiency and some kind of “good is good enough” approach in terms of quality. As part of using this technology, the choice of good de-Bayering algorithms is key, in particular to minimize the introduction of image disturbances like moiré, zipper artifacts and maze patterns, while maintaining as much information contents as possible. In real world scenarios, there are diverse influences than just the different sensor technology, which makes it very difficult to compare flights that did not take place under identical conditions. Since only the comparison of sharp images is meaningful, influences like contrast differences based on sun angle, atmospheric turbulences and the used method for motion compensation (Section 2.5) needs to be considered.

2.4 From CCD to CMOS technology

Since some years, many camera manufacturers are increasingly adopting CMOS sensors over traditional CCDs (Neumann et al., 2016). This shift is driven by CMOS technology catching up (and in most ways surpassing) CCD in image quality while offering key practical advantages (e.g. higher speed read-out, better dynamic range, lower power consumption, higher light sensitivity, etc.). The significantly higher light sensitivity of current CMOS sensors (e.g. Sony IMX 411 or SONY IMX 811)

compared to the latest CCDs in aerial cameras can roughly be quantified with a factor of two. For real world scenarios and with the assumption that the used aperture of the same lens was used, shorter exposure times can be used with even better signal noise ratio. While a CCD sensor would result in an exposure time of 1/500 s, a CMOS sensor will be able to use 1/1000 s while at the same time providing better image quality. Moreover CMOSs feature an improved chief ray angle tolerance which leads to a significant smaller light decrease towards the sensor edges. It is noteworthy that especially at too short exposure time the current algorithms provide visually good images (through denoising / histogram adjustment), while they might lose detail in texture (e.g. grass) and color stability when originally being underexposed. Having a sufficient amount of light to heat the sensor it is important for image quality, independent of the post-processing method. A challenge is that time delay and integration is not possible for CMOS sensors, raising the need for other approaches for motion compensation.

2.5 Motion compensation (MC) and exposure time

Motion compensation in aerial photogrammetry means the mitigation of image blur caused by the movement of the airplane (or camera) during image acquisition. There has been some debate in the community about the correct and best approaches to deal with motion compensation (Dohr et al., 2022) and shutter speeds. Requirements for image quality follow Modulation Transfer Function (MTF) measurements. Motion compensation is particularly important for multi-perspective cameras with great variations of “optical flow” in the image plane. Short exposure times may have negative effects on image quality especially under poor lighting conditions. At the same time, advanced approaches to motion compensation cannot do “magic”, i.e. if the blur becomes too large, it cannot be completely eliminated even by the most advanced image processing algorithms.

The diverse camera producers use different motion compensation approaches. Due to forward motion and rotational movements, blurring occurs in the images, as they must be captured from moving platforms. Blur negatively affects the resolution of the images and therefore it should be minimized using appropriate techniques. Full motion compensation addresses the effects of both forward motion and changes in camera rotation.

A comparable theoretical impact of forward (translational) and rotational motion is reported in Table 3. Values are computed for the Vexcel Ultracam Eagle 4.1 camera geometry, assuming a linear velocity typical for missions and a rotational motion of 2 deg/s, which may happen even for actively stabilized mounts. In this specific scenario, translational motion theoretically causes a blur of 1.6 pixels GSD, while the rotational component induces a blur of 1.4 pixels GSD. It's important to note that in practice, both types of motion will always occur simultaneously.

	Linear motion	Rotational motion
Velocity	80 m/s	2 deg/s = 70 m/s
Exposure time	1/1000 s	1/1000 s
Principal distance	150 mm	150 mm
GSD @ 1995 m	5 cm	5 cm
Image motion in object space	8 cm (1.6x GSD)	7 cm (1.4x GSD)

Table 3. Theoretical image motion for translational and rotational movements in aerial cameras.

The active compensation of image motion in airborne imaging was already addressed in the mid-1980s with the Zeiss Jena LMK1000 camera (Zeth and Voss, 1984). This camera was the first commercial mapping system in which forward motion

compensation (FMC) was applied mechanically by moving the film during exposure. A specialized mechanism integrated into the film cassettes enabled film movement at speeds of up to 30 mm/s. The precise compensation speed was determined by the ratio between velocity over ground and height above ground (v/h). If the imaged object in the focal plane is actively moved along with this scale-accurate speed, then no motion blur due to the sensor's forward motion occurs in the image.

Recognizing that this approach works only over flat ground and could not correct for rotational motion, stabilizing platforms were introduced concurrently in the 1980s. Unlike earlier passive mounts that only used bumpers to dampen high-frequency aircraft vibrations affecting the sensor, these active mounts additionally incorporated sensors to measure the true angular movements and actively compensate for them. The current Leica Geosystems PAV 80 stabilized mount, for example, offers a stabilization range of ± 7 deg for roll, -8 to $+6$ deg for pitch, and ± 30 degrees for drift. The stabilized mount is also important for achieving highly regular nadir block structures with precise overlaps as defined during the planning phase.

Figure 5 presents the angular rates at image exposures measured by GNSS/inertial sensors fixed to an actively stabilized, high-quality camera platform (SOMAG GSM4000 mount) during a typical, relatively smooth imaging flight. Despite the active mount's compensation for flight dynamics, residual angular rates persist. These rates, denoted in ω (ϕ), and κ (κ), exhibit variations (std.dev.) of approximately 0.3 deg/s (ω , ϕ) and 0.5 deg/s (κ) with peak values reaching up to 1.5 deg/s. In more turbulent flights, peak values of several deg/s can occur during camera exposure. For instance, an exemplarily flight captured 440 images with a Vexcel Dragon 4.1 camera. During the 1/1000 s exposure, this flight showed maximum angular rates of 7.6 deg/s (ω), 6.3 deg/s (ϕ) and 5.7 deg/s (κ), while the variations were 0.5 deg/s (ω , ϕ) and 1 deg/s (κ). For nadir imagery, the remaining rotational movements in ω and ϕ are directly projected into the image. In contrast, changes in κ influence the image borders more significantly than the centre. This data highlights that even sophisticated gyro-stabilized mounts, over short timeframes, cannot fully counteract motion, a consequence of the significant (around 70 kg) mass inertia of the camera.

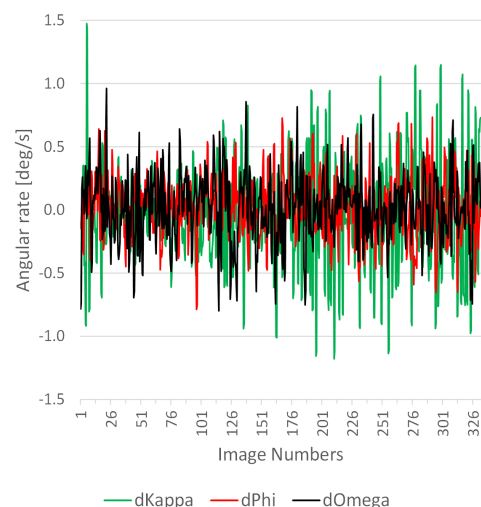


Figure 5. Angular changes in omega, phi, kappa [deg/s] at time of exposure, with active stabilized mount.

The influence of non-compensated rotational motion on image blur is depicted in Figure 6. The longer the exposure time, the greater the likelihood that angular motion will be the primary

source of image blur. This effect is supported by real-world data from a Vexcel Osprey 4.1 flight mission. Acquired during calm, near-ideal weather at a ground sampling distance of 5 cm, four distinct shutter speeds (1/1000s, 1/750s, 1/500s, and 1/250s) were used for each of the four flight lines, with the stabilized mount active. The results show that with exposure times of 1/500 s and longer, the angular image blur regularly exceeded one pixel.

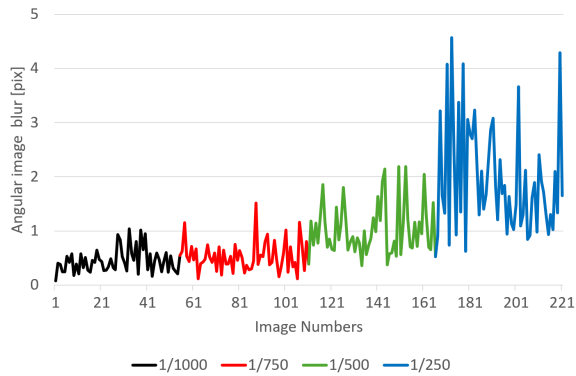


Figure 6. Impact of angular motion on image blur [pix].

Motion compensation now addresses both linear and rotational movement to ensure blur-free images. Fundamentally, there are two distinct concepts for motion compensation:

1. Primarily avoid motion in the images
2. Allow for a certain amount of motion blur and correct it afterwards in the images.

The traditional forward motion compensation by moving the film in combination with the stabilized mount belongs to the first concept, as most current methods applied in digital mapping cameras. In early cameras with CCD sensors, the movement of film principle was mimicked by shifting of charges from pixel to pixel as the image information moves in focal plane due to the forward motion (Time Delayed Integration - TDI). This TDI no longer works for CMOS sensors, as the individual neighbouring pixels on the sensor are not coupled directly. This is why the Leica DMC 4 camera now moves the sensor again - purely mechanically - like the original FMC in film cameras. The IGI Urbanmapper and Phase One PAS 880i cameras, also using CMOS sensors, implement a different technique. This method just takes advantage of the good radiometry of modern sensors by choosing very short exposure times and then brightening the slightly dark image in post-processing by histogram equalization. As this technique is therefore based on purely photographic principles it can be called photocentric motion control. On the other hand, the Adaptive Motion Compensation (AMC) method, as implemented in the latest Vexcel mapping sensors from generation 4.1, takes a different approach. AMC assumes that the blur in the images can be calculated out of the images using digital image processing afterwards, thus being the only current method following the concept (2) above. The approach relies on the assumption that a certain blur is accepted in the original image structure. If the original movement of the sensor during exposure, which is the reason for this image blur, is precisely known, the sharp image can be reconstructed from the blurred image by image restoration techniques (Segall & Katsaggelos, 2003; Dohr et al., 2022).

AMC can correct for all types of image blur but the result is very sensitive to the accuracy of the PSF / blur operator. All remaining methods, following concept (1) are limited by the three rotational changes of the sensor platform, that are not compensated by the stabilized mount. Any errors in the applied assumption of the forward motion will also affect this approach. The scale

variations in images due to differences of ground heights, i.e. terrain undulations and perspective distortions caused by image tilt have to be discussed separately. The perspective distortion can be corrected by the AMC approach. But effect of height variations impacts all the presented methods. Nevertheless, if height models are known a priori for the mission area, the local image scale changes can be integrated in the AMC approach.

3. Camera calibration

To achieve a well-calibrated aerial camera system, two fundamental approaches are widely adopted in the industry. The first is *laboratory calibration*, which involves calibrating the camera system in a controlled, well-defined, and stable laboratory environment. The second approach leverages *flight data calibration*, wherein well-structured aerial imagery and associated metadata (Ground Control Points – GCPs and/or GNSS/inertial exterior orientation measurements) are used to compute the camera's calibration parameters. These two methods can also be employed in combination to capitalize on their respective strengths. Each approach offers distinct advantages and limitations. Laboratory calibration benefits from a controlled setting that ensures high repeatability and is inherently free from external influences such as atmospheric refraction, Earth curvature or mapping projection distortions. This controlled environment enables robust estimation of key intrinsic parameters, including principal point location, focal length and lens distortion parameters. However, one of the challenges of laboratory setups is the relatively short object-camera distance compared to actual flight conditions. When a fixed-focus lens is used, this necessitates the use of a smaller aperture to achieve sufficient depth of field and image sharpness, especially for precise marker detection.

Conversely, flight-based calibration requires strict adherence to several data acquisition criteria to ensure high-quality results (Mueller et al., 2016). These include the execution of cross-flight patterns, inclusion of multiple GSDs, a dense network of accurately surveyed GCPs and high-precision GNSS/IMU data. In either calibration approach, the resulting parameters are, strictly speaking, valid only under the specific environmental conditions present at the time of calibration. But the variability in operating environments, such as temperature fluctuations during flight, presents a significant challenge. To address this, modeling approaches were proposed to compensate for such environmental variations and improve calibration robustness (Ladstädter et al., 2010). Nevertheless, these models and methods also have their limitations. Therefore, even for a well-calibrated camera system, it is sometimes necessary to introduce additional correction parameters during the bundle adjustment process. These corrections, when applied to a high-quality calibration, are typically on the order of sub-micrometer to one micrometer. As such, the expertise and judgment of the photogrammetrist remain critical in achieving the highest possible accuracy and reliability in photogrammetric products.

4. Oblique photogrammetry

Multi-view or multi-head or oblique cameras are of particular interest in the aerial mapping field as they provide more comprehensive coverage of complex environments, capturing images from multiple angles. This improves mapping accuracy in urban and other detailed settings, allows to boost 3D modelling processes and supports various smart city applications (Gruber and Walcher, 2013; Remondino and Gerke, 2015; Toschi et al., 2017;). After many years of developments and investigations,

oblique aerial photography is becoming the *de-facto* acquisition method for urban environment. The most interesting issues in oblique photogrammetry are afterwards reported.

4.1 GSD in oblique view

The 45 deg tilt of today's aerial oblique mapping cameras has several influences on the image GSD, that are way more complex than a simple scale variation from the front to the back of the oblique image (see also Figure 4 and Table 1). This simplified model holds true only when the camera's focal plane is parallel to the content on the ground, like rooftops which are also tilted of ca 45 deg. To account for real-life scenarios, three distinct GSD components must be considered:

- *Horizontal GSD*: it represents the pixel resolution projected onto the ground along the line of sight and is relevant for all features lying directly on the terrain, without elevation above it.
- *Vertical GSD*: it defines the pixel resolution on vertical surfaces, such as building facades.
- *Cross line of sight GSD*: it is similar to Horizontal GSD but is measured perpendicular to the viewing direction.

Each of these GSD components is influenced by the varying scale of oblique images. Notably, vertical GSD behaves differently compared to the others due to the counteracting effects of perspective foreshortening and viewing angle compensation, which help maintain a relatively consistent resolution across the image (Figure 7). On vertical surfaces, such as facades, this balance mitigates distortions. Most current sensors use longer focal lengths for the oblique cameras yielding similar GSDs in the centre of the oblique images as in the nadir ones. At the same time, longer focal lengths yield lower GSD variations in the images. Ideally the focal length ratio between oblique and nadir would be the square root of 2.

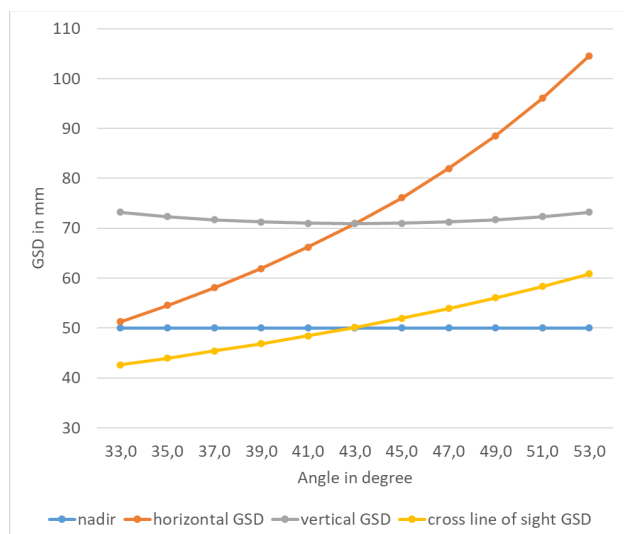


Figure 7: GSD curves wrt oblique angles for a 5 cm nadir GSD (blue line) with an ideal oblique-nadir focal length ratio of square root of 2.

4.2 Extra strips

Usually, tenders are asking for full oblique coverage of the surveyed area, which results in 5 different viewing directions being available for every single object. In case of a building this translates into full coverage of the facades as well as the roof (Figure 8). But, given the 45 degrees tilt of the oblique views, this implies extending the flight lines for the forward- and backward-

pointing cameras at both ends as well as adding extra strips for the left- and right-pointing cameras, i.e. extra flying time and costs. For the 45-degree tilt, the magnitude of the AOI extension is at the same order as the flight height above ground. Thus, cameras with larger focal lengths require a bigger extension than those with shorter focal lengths. Two examples are shown in Figure 9: a Leica City Mapper 2H (focal length of 146 mm for the nadir and 189 mm for the obliques) and a Vexcel UltraCam Osprey 4.1 (focal length of 80 mm for the nadir and 120 mm for the obliques), respectively. It is clearly visible that the longer the focal lengths, the bigger are the distances between the individual footprints of a given exposure, requiring more additional lines to achieve a full 3D coverage.

The shape of the footprints depends on the sensor design (size and orientation of the CMOS chip(s) within the field of view of the lenses).

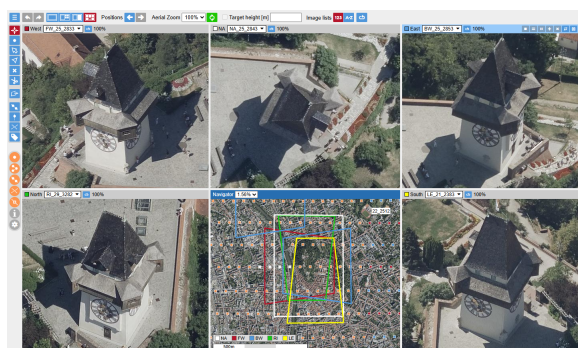


Figure 8: The Clock Tower (Uhrturm) in Graz (Austria) seen in the oblique views from cardinal directions (Vexcel UltraCam Osprey 4.1, 2022; AVT Measuree viewer - <https://measuree.at>).



Figure 9: Footprints of the nadir and oblique cameras of a single exposure taken with a City Mapper 2H at 10 cm GSD over Luxembourg (left) and with an UltraCam Osprey 4.1 at 2.5cm GSD over Speyer, Germany (right). The longer focal lengths of the Leica sensors lead to bigger separations between the footprints.

4.3 Tie point extraction

Compared to standard APM in nadir-only image blocks, tie points extraction is more challenging when different viewing directions should be matched (Toschi et al., 2018). The main challenge for tie-point extraction in multi-perspective image blocks is their difference in appearance due to their physical characteristics and the change of perspective and lighting. In case of large oblique blocks and long focal lengths, the time interval between recordings of the same section in object space may also become an issue.

Matching methods can extract keypoints in all images (nadir and obliques) and then try to correlate them across all views. Alternatively, given a set of keypoints extracted on selected

(generally nadir) master images, the search for correspondences in the overlapping images is guided from object space. Modern software systems extending tie point extraction with a focus on oblique imagery should be used, in order to use additional methods for filtering tie points. These tools consider more than the reprojection error (which increases for perspective change), to achieve a well distributed tie point distribution in the block and connect also oblique strips to Nadir and between each other. This way, all view directions can be robustly and accurately aligned with each other. Even with an increased average reprojection error, a good relative accuracy and high accuracy on ground can be achieved.

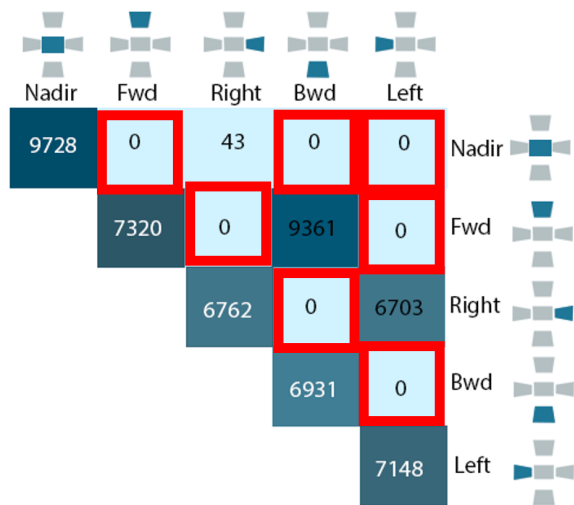


Figure 10: Example of low connectivity between nadir and oblique views (Farella et al., 2025).

Model	Manufacturer	LiDAR unit					Camera unit			
		Laser wavelength [µm]	PRF [kHz]	FOV [°]	Scan pattern	Vertical accuracy [cm]	#channels	Spectral bands	Image res. [MP]	Focal length [mm]
Country Mapper	Hexagon/Leica	1064	2000	10-60	Oblique	< 5 (1 σ)	1	RGB-NIR	~424	-
City Mapper2	Hexagon/Leica	1064	2000	20-40	Oblique	< 5 (1 σ)	2 nadir + 4 oblique	RGB(nadir), NIR(nadir), RGB(obliques)	150	• V2L [71,71,112] • V2S [112,71,148] • V2R [146,71,189]
Terrain Mapper-3	Hexagon/Leica	1064	2000	10-60	Circular, elliptical, skew elliptical	< 5 (1 σ)	1	RGB-NIR	150	71,71
SPL100	Hexagon/Leica	532	6000	20-30-60	Circular	< 10	1	RGB-NIR	80	50,80,150
Chiroptera 4X	Hexagon/Leica	512/1064	500/140	28/40	Elliptical	< 5 (topo)	1	RGB-NIR	80	50
HawkEye 4X	Hexagon/Leica	512/1064	500/140/40	28/40	Elliptical	< 5 (topo)	1	RGB-NIR	80	50
VQ-1560-DW	RIEGL	532/1064	2x1000	58	Cross lines btw channels	2	2	RGB-NIR	Up to 150	35,50,80
CP-780	RIEGL	1064	1000	60	Parallel lines	2	2	RGB-NIR	100	50
VQ-880-GII	RIEGL	532/1064	700/900	40	Circular/curved parallel lines	2.5	Up to 2	RGB and/or IR	100	50
VQ-840-G	RIEGL	532	100	40	Elliptic	1.5	1	RGB	12	50
Galaxy T2000	Teledyne Optech	1064	2000	10-60	Sawtooth	< 5	1-4	RGB-NIR	150	50,70
Eclipse	Teledyne Optech	1550	450	60	Parallel lines	< 5	1	RGB	30	35
Titan	Teledyne Optech	532/1064/1550	900 (total)	60	Lines	< 5	Up to 2	RGB/NIR	29/80	-
CZML Nova	Teledyne Optech	532/1064	10/80	40	Circular	< 15 (2 σ)	2	RGB/hyperspectr.	100	-
LiMMapper-7800VQ	IGI	1064	1000	60	Parallel lines	2	Up to 5	RGB/NIR	150	40,50
LiMMapper-4800VQ	IGI	1550	2000	75	Parallel lines	< 5 (topo)	Up to 5	RGB/NIR	150	32,40,50
LiMMapper-1560VQ	IGI	1000	2x1000	60	Cross lines btw channels	2	Up to 2	RGB/NIR	150	40,50
LiMMapper-1560VQ	IGI	1064	2000	75	Parallel lines	2	Up to 5	RGB/NIR	150	32,40,50
Ultracam DRAGON 4.1	Vecell	1052	2400	40-60	Parallel lines	2	5	RGB(nadir), NIR(nadir), RGB(obliques)	150	• 80,123 • 50,80

Table 4: Some of the existing hybrid aerial sensors.

5. Hybrid sensors

Another recent trend is the wider usage of hybrid sensors (Table 4), i.e. the combination of classic metric mapping cameras with aerial LiDAR sensors. It is quite obvious that this integration is somehow a compromise, when just taking the amount of individual camera and LiDAR systems into account. In terms of pure quality and efficiency, the individual systems are superior.

But there are benefits from simultaneous collection which have not been fully exploited so far. Without hybrid systems an aircraft with two hatches is needed as well as two individual sensor systems with the corresponding periphery (gyro-stabilized mount, IMU). Moreover, the lack of efficient and reliable concurrent image and LiDAR data processing is still limiting the potential of hybrid aerial sensors. Cledat and Skaloud (2020) reviewed various methods for joint LiDAR and image matching. In general methodologies try to correct point cloud errors caused by an imperfect trajectory determination, relying on constraints either on the optical data, i.e. spatial constraints (Glira et al., 2019; Jonassen et al., 2023), or on the navigation data, i.e. temporal constraints (Cucci et al., 2017; Mouzakidou et al., 2022).

6. Conclusions and recommendations

The paper presents actual trends and challenges in aerial 3D mapping. Our take-away messages could be summarized as:

- Collection efficiency has become the leading parameter - in opposite to quality - and software still needs many improvements to produce high quality 3D data from the acquired data. Indeed, short update cycles become ever more important and tend to overrule other quality requirements like accuracy, optimal radiometry, high sun angles, or imagery free of clouds and/or cloud shadows.
- Adapting standard hardware for photogrammetric flights, such as medium format frames with Bayer pattern sensors enabled the combination of many sensors and higher productivity.
- To leverage the increased productivity, it is recommended to adjust the GSD to smaller (i.e., better) values, to compensate for losses (due to higher altitude / increased atmospheric loss, smaller pixels, Bayer pattern interpolation etc. – e.g. by 20%) and/or limit flight altitude to reach reasonable radiometric conditions.
- To achieve high completeness in DSM generation, it has become common practice to capture at 80% forward overlap as no additional costs in terms of flight time is required (with state-of-the-art sensors), while providing additional completeness and accuracy in the final products.
- Using balanced focal lengths allows efficient data capturing and derivation of detailed 3D information (through manual stereo or automatic elevation / mesh generation), notwithstanding realistic true ortho results. For the latter, a high forward (80%) and medium sideward overlap (60% or more) should be considered for optimal results. A True ortho computation leveraging the DSM and its completeness allows the removal of remaining building lean effects.
- Using motion compensation allows for longer exposure times and better radiometric results (texture and color) - for high resolution and high flying speed it is even required to achieve sharp imagery.
- Oblique imagery is important for high resolution facade information, detailed 3D city modeling or industrial applications - although they find applications also in statewide coverage.
- Hybrid camera/LiDAR sensors are gaining attention as capable of providing both data modalities and extending the application, e.g. through better DTMs through penetrating vegetation, capturing powerlines and for completing gaps of image-matching point clouds in presence of narrow street canyons.
- Another issue related to flying height refers to aircraft design: The practical limit for flying with non-pressurized aircraft is around 5000 m, depending on the fitness and willingness of

the crew. It is recommended to use bottled oxygen above 3500 to 4000 m. But flying for long times with oxygen masks may be very cumbersome. Greater flying heights can be achieved with pressurized aircraft. The protective glass below the camera required for such aircraft usually has a measurable effect on image geometry (in the μm domain and, thus, at pixel level). Depending on glass quality, thickness and stability, self-calibration may be necessary for such solutions.

- In camera calibration processes, due to the actual higher flying heights, temperature and pressure should also be taken into consideration to retrieve stable interior orientation results.
- Relative sensor position and boresight information requires refinement from the field using ground control as data provided from labs are generally not sufficient to achieve accurate 3D results.

References

- Bacher, U., 2022. Hybrid aerial sensor data as basis for a geospatial digital twin. *Int. Arch. Photogramm. Remote Sens. Spatial Inf. Sci.*, 43, 653-659.
- Cucci, D.A., Rehak, M., Skaloud, J., 2017. Bundle adjustment with raw inertial observations in UAV applications. *ISPRS J. Journal of Photogrammetry and Remote Sensing*, 130, pp. 1-12.
- Dohr, S., Muick, M., Schachinger, B., Gruber, M., 2022. Image motion compensation – the Vexcel approach. *Int. Arch. Photogramm. Remote Sens. Spatial Inf. Sci.*, XLIII-B1-2022, 333-338.
- Farella E.M., Morelli L., Remondino F., Qin R., Schachinger B., Legat K., 2025. Investigating the new Ultracam Dragon hybrid aerial mapping system. *Int. Arch. Photogramm. Remote Sens. Spatial Inf. Sci.*, XLVIII-M-6-2025, 117-125.
- Glira, P., Pfeifer, N., Mandlbürger, G., 2019. Hybrid orientation of airborne LiDAR point clouds and aerial images. *ISPRS Annals of the Photogramm. Remote Sens. Spatial Inf. Sci.*, 4, 567-574.
- Goodbody, T.R.H., Coops, N.C., White, J.C., 2019. Digital aerial photogrammetry for updating area-based forest inventories: a review of opportunities, challenges, and future directions. *Curr Forestry Rep.*, 5, 55-75.
- Gruber M., Walcher, W., 2013. Oblique Image Collection -- Challenges and Solutions. *Proc. Photogrammetric Week 2013*.
- Haala, N., Kölle, M., Cramer, M., Laupheimer, D., Zimmermann, F., 2022. Hybrid georeferencing of images and LiDAR data for UAV-based point cloud collection at millimetre accuracy. *ISPRS Open J. Photogrammetry and Remote Sensing*, 4:1-11.
- Hinz, A., Dorstel, C., Heier, H., 2001. DMC - The digital sensor technology of Z/I-Imaging. *Proc. Photogrammetric Week*.
- Ladstädter, R., Tschammerneegg, H., Gruber, M., 2010. Calibrating the Ultracam aerial camera systems - an update. *Int. Arch. Photogramm. Remote Sens. Spatial Inf. Sci.*, XXXVIII.
- Lehtola, V.V., Koeva, M., Oude Elberink, S., Raposo, P., Virtanen, J.P., Vahdatikhaki, F., 2022. Digital twin of a city: Review of technology serving city needs. *Int. Journal of Applied Earth Observation and Geoinformation*, Vol. 114, 102915.
- Jacobsen, K., Ladstädter, R., Bosch, R. 2025. Geometric Accuracy of PhaseOne PAS Pana. *Int. Arch. Photogramm. Remote Sens. Spatial Inf. Sci.*, XLVIII-M-6-2025.
- Jonassen, V.O., Kjorsvik, N.S., Gjevestad, J.G.O., 2023. Scalable hybrid adjustment of images and LiDAR point clouds. *ISPRS Journal of Photogrammetry and Remote Sensing*, 202, 652-662.
- Kocaman, S., Akca, D., Poli, D., Remondino, F., 2022. *3D/4D City Modelling - From Sensors to Applications*. Whittles Publishing, 224 p.
- Megahed, Y., Shaker, A., Yan, W.Y., 2021. Fusion of airborne LiDAR point clouds and aerial images for heterogeneous land-use urban mapping. *Remote Sensing*, 13(4), p.814.
- Mouzakidou, K., Brun, A., Cucci, D. A., Skaloud, J., 2024. Airborne sensor fusion: Expected accuracy and behavior of a concurrent adjustment. *ISPRS Open Journal of Photogr. and Rem. Sens.*, 12, 100057.
- Mouzakidou, K., Cucci, D. A., Skaloud, J., 2022. On the benefit of concurrent adjustment of active and passive optical sensors with GNSS & raw inertial data. *ISPRS Annals of the Photogramm. Remote Sens. Spatial Inf. Sci.*, V-1-2022, 161-168.
- Mueller, C., Neumann, K., 2016. Leica DMC III calibration and geometric sensor accuracy. *Int. Arch. Photogramm. Remote Sens. Spatial Inf. Sci.*, XL-3/W4, 1-9.
- Neumann, K., Welzenbach, M., Timm, M., 2016. CMOS imaging sensor technology for aerial mapping cameras. *Int. Arch. Photogramm. Remote Sens. Spatial Inf. Sci.*, XLI-B1, 69-72.
- Poli, D., Moe, K., Legat, K., Toschi, I., Lago, F., Remondino, F., 2017. Use of vertical aerial images for semi-oblique mapping. *Int. Arch. Photogramm. Remote Sens. Spatial Inf. Sci.*, Vol. XLII-1-W1, 493-498.
- Remondino, F., Toschi, I., Gerke, M., Nex, F., Holland, D., McGill, A., Lopez, J.T., Magarinos, A., 2016. Oblique Aerial Imagery for NMA - Some Best Practices. *Int. Arch. Photogramm. Remote Sens. Spatial Inf. Sci.*, XLI-B4, 639-645.
- Remondino, F., Gerke, M., 2015. Oblique aerial imagery: a review. *Proc. Photogrammetric Week*, 75-83.
- Remondino, F., Spera, M.G., Nocerino, E., Menna, F., Nex, F.C., 2014. State of the art in high density image matching. *Photogrammetric Record*, 29, 144-166.
- Rupnik, E., Nex, F.C., Toschi, I., Remondino, F., 2014. Aerial multi-camera systems: accuracy and block triangulation issues. *ISPRS J. Photogrammetry and Remote Sensing*, 101, 233-246.
- Segall, C. Andrew & Katsaggelos, Aggelos K. 2003. Digital Image Restoration—Classical. *Encyclopedia of Optical Engineering*, 1:1, 411-427.
- Stathopoulou, E.K., Remondino, F., 2023. A survey of conventional and learning-based methods for multi-view stereo. *Photogrammetric Record*, Vol. 38(183), 374-407.
- Toschi, I., Remondino, F., Hauck, T., Wenzel, K., 2019. When photogrammetry meets LiDAR: Towards the airborne hybrid era. *GIM International*, 17-21.
- Toschi, I., Remondino, F., Rothe, R., Klimek, K., 2018. Combining airborne oblique camera and LiDAR sensors: Investigation and new perspectives. *Int. Arch. Photogramm. Remote Sens. Spatial Inf. Sci.*, XLII-1, 437-444.
- Toschi, I., Ramos, M.M., Nocerino, E., Menna, F., Remondino, F., Moe, K., Poli, D., Legat, K., Fassi, F., 2017. Oblique photogrammetry supporting 3D urban reconstruction of complex scenarios. *Int. Arch. Photogramm. Remote Sens. Spatial Inf. Sci.*, XLII-1-W1, 519-526.
- Zeth, U., Vess, G., 1984. Some aspects of forward motion compensation in an aerial camera. *Int. Arch. Photogramm. Remote Sens.*, Vol XXV, pp. 339-350.